JOURNAL OF APPLIED ELECTROCHEMISTRY 24 (1994) 676–684

A three-segment electrodiffusion probe in axisymmetric flow with stagnation and separation

F. BALERAS, C. DESLOUIS, B. TRIBOLLET

UPR 15 du CNRS, 'Physique des Liquides et Electrochimie', Université P. et M. Curie, 4 place Jussieu, 75252 Paris Cédex 05, France

V. SOBOLIK

Institute of Chemical Process Fundamentals, Academy of Sciences of the Czech Republic, 16502 Prague 06, Czech Republic

Received 13 July 1993; revised 21 December 1993

Calculation is presented of the influence of the normal velocity component on the directional characteristics of a three-segment electrochemical probe in the vicinity of a stagnation or a separation point. The results obtained here for a 2D flow corresponding to an axisymmetric flow having a stagnation point show quantitative differences, especially in the stagnation region, with respect to an earlier calculation performed on a 2D flow corresponding to a planar flow having a stagnation line. An experimental study with such a probe is then reported which demonstrates the possibility of this arrangement in the stagnation region of an immersed jet.

1. Introduction

The three-segment electrodiffusion probe has been recently developed to study liquid flow close to a wall (for example, see [1–4]). From the three measured diffusion currents of a three-segment probe, more information about the flow field than the two components of the velocity gradient at the wall can be obtained. Wein and Sobolik [5] calculated the influence of the velocity normal to the wall on the directional characteristics (i.e. the dependence of the elementary currents of the segments on the flow direction) in the case of a 2D planar flow with stagnation. Sobolik *et al.* [6] experimentally confirmed these results with a three-segment electrode flush mounted in a rotating disc.

In real flow situations, the local velocity distribution near the wall can be more complicated than a two-dimensional one. An example of such a situation is the flow in a bubble column induced by a bubble passing the wall. It is anticipated that the 2D flows (axisymmetric or planar) with stagnation are asymptotic cases of real flows from the view point of the influence of a normal velocity component on the directional characteristics.

However, as it is not justified to apply the results established for a 2D planar flow situation [6] to a 2D axisymmetric flow situation, we describe, in this paper, a study of the directional characteristics in radial axisymmetric flow with stagnation. Probe inertia will not be considered here as only steady or quasisteady conditions are implied. In a second part, the flow in the stagnation region of an immersed jet is studied with a three-segment probe.

This paper was presented at the International Workshop on Electrodiffusion Diagnostics of Flows held in Dourdan, France, May 1993.

2. Theoretical background

A fluid stream with a circular cross section impinges on a wall orthogonally to its surface, and then flows radially parallel to the wall. Such a case occurs near a stagnation point of a body of revolution in a flow parallel to its axis. The problem is defined in cylindrical coordinates (r, ϕ, z) (see Fig. 1). According to Prandtl's boundary layer theory, a potential flow with velocities $U(r)$ and $W(z)$ and a boundary layer flow with $v_r(r, z)$ and $v_z(r, z)$ can be defined [7], with

$$U = ar \quad \text{and} \quad W = -2az \tag{1}$$

and

$$\begin{cases} v_r = 1.312(a^3/\nu)^{1/2} zr = Azr \\ v_z = -1.312(a^3/\nu)^{1/2} z^2 = -Az^2 \end{cases} \tag{2}$$

and the boundary conditions

$$\begin{aligned} v_z = v_r = 0 \quad & \text{for } z = 0 \\ v_r = U \quad & \text{for } z \longrightarrow \infty \end{aligned} \tag{3}$$

The boundary layer thickness defined as $\delta_h = 2(\nu/a)^{1/2}$ does not depend on the distance from the stagnation point and the electrode placed in the stagnation point is so-called uniformly accessible.

The wall velocity gradient then reads:

$$q = \frac{\partial v_r}{\partial z} = Ar \tag{4}$$

It follows, from Equations 2 and 4, that the wall velocity gradient is proportional to a constant A and the normal velocity component is equal to the

0021-891X 1994 Chapman & Hall

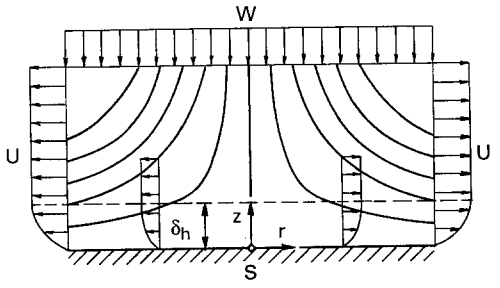

Fig. 1. Stagnation region in axisymmetric flow.

product of this constant and the squared distance from the wall with a negative sign.

From the velocity distribution, it is possible to solve the convective diffusion equation. After Acrivos [8], Newman calculated [9] the expression for the local limiting current density on an electrode embedded in an axisymmetric body (see Fig. 2):

$$i_d = \frac{nFc(D/3)^{2/3}}{\Gamma(4/3)}\left[\int_0^x |q|^{1/2} r^{3/2}\,dx\right]^{-1/3} (|q|r)^{1/2} \quad (5)$$

where both r and q are functions of the integration variable x which has its origin at the leading edge of the electrode. Without changing the value of the integral in Equation 5, a new x coordinate can be defined as the curvilinear coordinate with its origin at the stagnation point (or separation point if the Reynolds number is low enough, as the flow may be reversed in Fig. 2). This change provides an obvious simplification since in the following, a plane surface, instead of a body of revolution, is considered. For example, for an axisymmetric jet impinging on a wall, $r = x, q = Ar$ and the limiting current density takes the following form:

$$i_d(r) = \frac{nFc(D/3)^{2/3}}{\Gamma(4/3)}\left[\int_{r_0}^r A^{1/2} x^2\,dx\right]^{-1/3} A^{1/2} r \quad (6)$$

with the forward edge of the electrode in r_0.

When the stagnation point is located on the microelectrode area, then

$$i^* = \frac{nFc(D^2A/3)^{1/3}}{\Gamma(4/3)} \quad (7)$$

represents the local current density (because $r_0 = 0$) and the electrode is uniformly accessible from the standpoint of mass transport.

Equation 6 can be written as

$$i_d(r) = i^*\left[1 - \left(\frac{r_0}{r}\right)^3\right]^{-1/3} \quad (8)$$

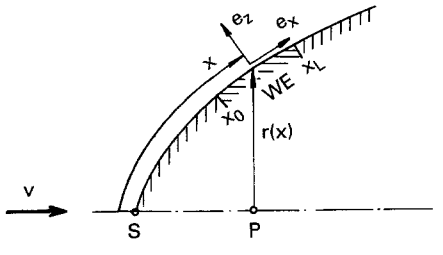

Fig. 2. Electrode (WE) placed on an axisymmetrical body.

3. Directional characteristics of radial segments on circular electrodes

3.1. *Forward critical region* A > 0

A circular electrode of radius R, with its centre at a distance h from the stagnation point, and its surface element, which will be used for the calculation of quadrature, are shown in Fig. 3. By integration of Equation 8, the limiting current density on the electrode is obtained as [10]

$$i_0 = \frac{2}{\pi R^2}\int_0^{\Psi_t}\int_{r_1}^{r_3} r i_d\,dr\,d\Psi$$

$$= \frac{2i^*}{\pi R^2}\int_0^{\Psi_t}\int_{r_1}^{r_3} \frac{r^2}{(r^3 - r_1^3)^{1/3}}\,dr\,d\Psi$$

$$i_0 = \frac{i^*}{\pi R^2}\int_0^{\Psi_t} [r_3^3(\Psi) - r_1^3(\Psi)]^{2/3}\,d\Psi \quad (9)$$

As the nature of the flow is not specified in the above calculations, Equation 9 also holds for the separation region. However, at the separation point itself, the theory does not apply.

The following relations (see Fig. 3) and the calculation of the current through the denoted segments, Equation 7, were used for the numerical treatment of Equation 9:

$$\left.\begin{aligned} &\sin\Psi_t = R/h, \quad \beta_t = \pi/2 - \Psi_t \\ &r_{1,3} = h[\cos\Psi \mp \{\cos^2\Psi - 1 + (R/h)^2\}^{1/2}] \\ &r_2 = h\sin\beta/[\sin(\pi - \Psi - \beta)] \end{aligned}\right\} \quad (10)$$

For $R = h$, i.e. when the stagnation point lies on the edge of the electrode, the calculated value of the limiting current density is equal to i^*. The results for the total current are compared to those previously obtained from 2D planar flow in Table 1. i_0 is the current density in an axisymmetric flow from Equation 9, i_p is the limiting current density in a 2D planar flow, after Wein and Sobolik [5] defined by

$$i_p/i_{Lp} = 1 - 2\kappa^2/99 - \kappa^4/309 \quad (11)$$

i_{Lp} is the limiting current density according to Lévêque [11] with the velocity gradient defined in the centre of the probe and a 2D planar flow:

$$i_{Lp} = 1.114(h/R)^{1/3} i^* \quad (12)$$

Using the velocity gradient of the 2D axisymmetric flow, the Lévêque current density is

$$i_{L0} = 0.884(h/R)^{1/3} i^* \quad (13)$$

The parameter κ is defined later in Equation 18.

Now, the circular electrode is segmented into several circular sectors, separated by infinitely thin insulating gaps. The directional characteristics, which represent the dependence of the normalized currents on each segment (with respect to the total current) as functions of the angle between the main flow direction and an arbitrarily prescribed reference radius of the probe, will be calculated in a similar

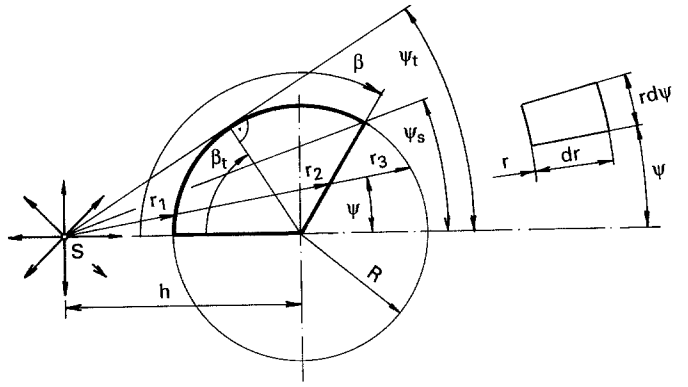

Fig. 3. Electrode near the stagnation point with the symbols used for the calculation of the current on a radial segment.

way to that described by Wein and Sobolik [5] and Deslouis *et al.* [4]. As a first step, the current $I(\beta)$ through a segment having an apex angle β and one arm directed to the stagnation point, as schematized in Fig. 3, is determined. Then, the current on a sector of angle 2α, with its bisector making an angle $\theta+\alpha$ with the flow direction, can be deduced as follows: as an example, for $\theta+2\alpha<\pi$, the current $I(2\alpha)=I(\theta+2\alpha)-I(\theta)$. Therefore, by symmetry considerations and algebraic combinations of currents, the current on any arbitrary segment can be calculated.

From Fig. 3, two cases must be distinguished according to the value of β:

$$\left.\begin{aligned} I_{s1} &= 2i^*\int_0^{\Psi_s}(r_2^3-r_1^3)^{2/3}\,d\Psi \qquad \text{for } \beta\leqslant\beta_t \\ I_{s2} &= I_{s1}+2i^*\int_{\Psi_s}^{\Psi_t}(r_3^3-r_1^3)^{2/3}\,d\Psi \quad \text{for } \beta>\beta_t \end{aligned}\right\} \tag{14}$$

The results will be given later together with the results corresponding to separation region.

3.2. *Rear critical region* A < 0

The flow in the opposite direction to that in Fig. 1 is now considered. This situation is less usual but a boundary layer flow, as described by Equation 2 with $A<0$, may exist, e.g. in the flow around a sphere at low Reynolds numbers. The point S is the separation point. The probe near the separation point is shown in Fig. 4. For calculation of the limiting current density, Equation 5 will be used again. The distance x is measured in the flow direction. The leading edge of the electrode $r_3(\Psi)$ is the origin of the x direction. The following relations then hold:

$$r(x)=r_3(\Psi)-x, \qquad |q|=-Ar \tag{15}$$

The limiting current density is

$$i_d=i^*\left[\left(\frac{r_3}{r}\right)^3-1\right]^{-1/3} \tag{16}$$

The limiting current through the whole electrode, calculated by numerical integration, does not depend on the flow direction and is given in Table 1. The directional characteristics were calculated by means of the combinations of the currents through the segments shown in Fig. 4.

The following relations were used:

$$\left.\begin{aligned} I_{s1} &= 2i^*\int_0^{\Psi_s}(r_3^3-r_2^3)^{2/3}\,d\Psi \qquad \text{when } \beta\geqslant\beta_t \\ I_{s2} &= I_{s1}+2i^*\int_{\Psi_s}^{\Psi_t}(r_3^3-r_1^3)^{2/3}\,d\Psi \quad \text{when } \beta<\beta_t \end{aligned}\right\} \tag{17}$$

Wein and Sobolik [5] and Sobolik *et al.* [6] have introduced a parameter κ which expresses the ratio of the maximum difference of the velocity gradient at the centre and the boundary of the probe and the wall gradient at the centre of the probe. Using the same definition, κ is redefined for the stagnation region:

$$\kappa=\delta q/q=AR/Ah=R/h \tag{18}$$

For the separation region, the difference has the

Table 1. Limiting current of a circular electrode as function of the distance from the stagnation point. The different current densities were defined in Equations 9, 11–13 and in references [5] and [11]

R/h	i_0/i^*	i_p/i^*	i_{L0}/i_0	i_{Lp}/i_p
0.1	1.907	2.400	0.999	1.000
0.2	1.519	1.903	0.995	1.001
0.3	1.335	1.661	0.990	1.002
0.4	1.223	1.507	0.982	1.003
0.5	1.147	1.396	0.971	1.005
0.6	1.093	1.311	0.959	1.008
0.7	1.055	1.241	0.944	1.011
0.8	1.027	1.183	0.927	1.014
0.9	1.009	1.132	0.908	1.019
1.0	1	1.088	0.884	1.023

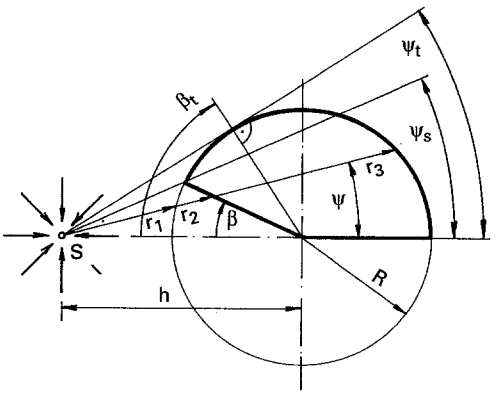

Fig. 4. Electrode near a separation point. Same symbols as in Fig. 3.

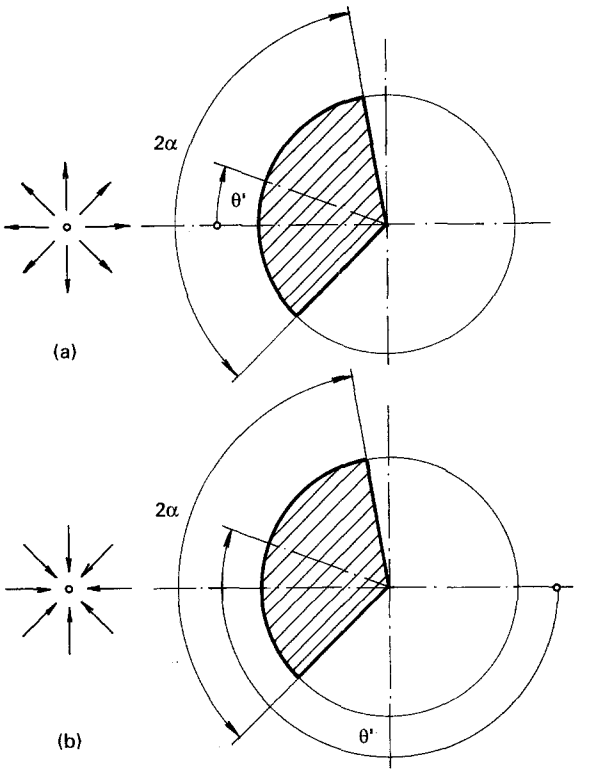

Fig. 5. Meaning of the segment angle 2α and flow angle θ: (a) Near a stagnation point, (b) near a separation point.

opposite sign and

$$\kappa = \delta q/q = -AR/Ah = -R/h \qquad (19)$$

By numerical integration of Equations 9, 14 and 17 the directional characteristics can be obtained, i.e. the dependence of the normalized current through a segment of angle 2α on the flow angle θ. The flow angle θ is defined as the angle between the flow direction at the centre of the electrode and the axis of the segment (see Fig. 5). The dependence of the directional characteristics on the value of κ, for $\alpha = \pi/3$ as an example (three-segment electrode), is shown in Fig. 6.

When the flow is towards the wall, the differential current between the front and rear segments decreases, and the directional characteristics are flattened, whereas when the flow is away from the wall, this difference increases up to $\kappa = -0.75$. For $\kappa < -0.75$, i.e. very close to the separation point, the influence of the radial flow, which transports fresh liquid to the rear segment, dominates the influence of the normal flow and the directional characteristics are flatter as κ becomes smaller.

The directional characteristics were fitted by the Fourier series:

$$\frac{I(\alpha,\theta,\kappa)}{\pi R^2 i^*} = \frac{\alpha}{\pi} + \sum_{m=1}^{n} C_m^{\mathrm{A}}(\kappa)\sin(m\alpha)\cos(m\theta) \qquad (20)$$

In fact, when $\kappa = \pm 1$, the directional characteristics must be totally flat because, for symmetry reasons, the current on each segment is proportional to the segment angle 2α and is not influenced by the concentration distribution over the other segments. Therefore, $\sum_{m=1}^{n} C_m^{\mathrm{A}}(\kappa)\sin(m\alpha)\cos(m\theta) = 0$ whatever the values of α and θ which means that the $C_m^{\mathrm{A}}(\pm 1)$ coefficients are all zero. The coefficients $C_m^{\mathrm{A}}(\kappa)$ for κ values different from ± 1 are given in Table 2.

For practical use, it is convenient to express the coefficients C_m^{A} as functions of coefficients C_m (see Wein and Sobolik [5]) and coefficients K_m containing the influence of the normal component:

$$C_m^{\mathrm{A}} = C_m K_m(\kappa)$$
$$= C_m(1 - E_{1m}\kappa - E_{2m}\kappa^2 - E_{3m}\kappa^3 - E_{4m}\kappa^4)$$

The values of C_m and E_{nm} are given in Table 3.

4. Discussion

The definition of κ determined from the geometry (see Equations 18 and 19) is the same for planar and axisymmetric flows with stagnation or separation, i.e. the velocity gradient depends linearly on the distance from the stagnation (or separation) point. However, there is a substantial difference in the structure of the flows. From the equation of continuity, more fresh solution approaches the probe from the normal direction in the axisymmetric flow with

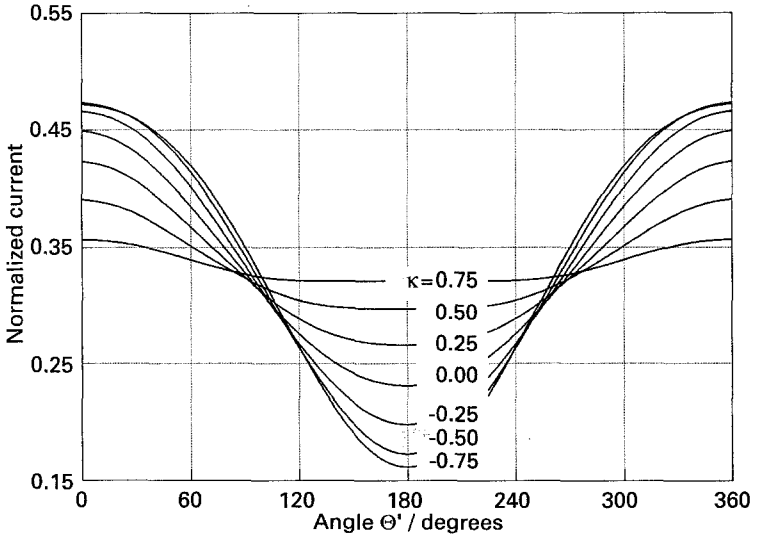

Fig. 6. Influence of the normal velocity component on the directional characteristics (normalized currents) in an axisymmetric flow, with $\alpha = \pi/3$ (three-segment electrode).

Table 2. Coefficients C_m^A

κ	C_1^A	C_2^A	C_3^A	C_4^A	C_5^A	C_6^A
−0.9	0.17620	−0.02238	0.00593	−0.00198	0.00070	−0.00023
−0.8	0.17968	−0.02083	0.00443	−0.00091	0.00003	0.00014
−0.7	0.18020	−0.01825	0.00263	0.00006	−0.00037	0.00021
−0.6	0.17823	−0.01499	0.00084	0.00075	−0.00045	0.00007
−0.5	0.17402	−0.01130	−0.00076	0.00109	−0.00030	−0.00012
−0.4	0.16779	−0.00738	−0.00204	0.00110	−0.00002	−0.00026
−0.3	0.15970	−0.00343	−0.00293	0.00084	0.00028	−0.00029
−0.2	0.14993	0.00039	−0.00339	0.00040	0.00050	−0.00020
−0.1	0.13867	0.00392	−0.00341	−0.00013	0.00058	−0.00003
0.0	0.12614	0.00702	−0.00303	−0.00064	0.00050	0.00015
0.1	0.11256	0.00953	−0.00230	−0.00103	0.00029	0.00027
0.2	0.09821	0.01136	−0.00133	−0.00124	0.00000	0.00029
0.3	0.08336	0.01241	−0.00021	−0.00120	−0.00028	0.00020
0.4	0.06835	0.01261	0.00090	−0.00094	−0.00048	0.00003
0.5	0.05353	0.01194	0.00185	−0.00047	−0.00053	−0.00016
0.6	0.03929	0.01041	0.00248	0.00009	−0.00038	−0.00026
0.7	0.02608	0.00811	0.00263	0.00060	−0.00008	−0.00020
0.8	0.01445	0.00524	0.00218	0.00085	0.00024	−0.00001
0.9	0.00518	0.00219	0.00114	0.00063	0.00033	0.00017

Table 3. Coefficients C_m and E_{nm}

m	*1*	*2*	*3*	*4*	*5*
C_m	0.1261	0.0070	−0.0030	−0.0006	0.0005
E_{1m}	1.045	−3.930	1.646	−4.759	0.717
E_{2m}	0.412	4.220	5.604	8.350	9.452
E_{3m}	−0.358	2.481	−3.200	9.406	−1.001
E_{4m}	−0.080	−1.477	3.627	−10.50	−12.14

stagnation than in the planar one. Therefore, the directional characteristics in axisymmetric flow with stagnation are flatter than in planar flow (compare Figs 6 and 7).

The directional characteristics display maximum variation for $\kappa = -0.75$ in axisymmetric flow. For $\kappa < -0.75$, i.e. for the electrode very close to the separation point, the trailing effect of the forward segment is not as strong as the flow of fresh solution in the radial direction on the rear segment, i.e. the segment closer to the point of separation. The following simulation was done to estimate the errors which may occur when planar theory is used to evaluate the data measured with the three-segment probe in an axisymmetric flow with separation. For different given values of κ, the directional characteristics were calculated for axisymmetric flow and these characteristics were then fitted by the formula established for planar flow. The resulting κ_p values for planar flow are shown in Fig. 8.

5. Application to flow mapping in an impinging jet cell

Confirmation of the above theory was attempted by

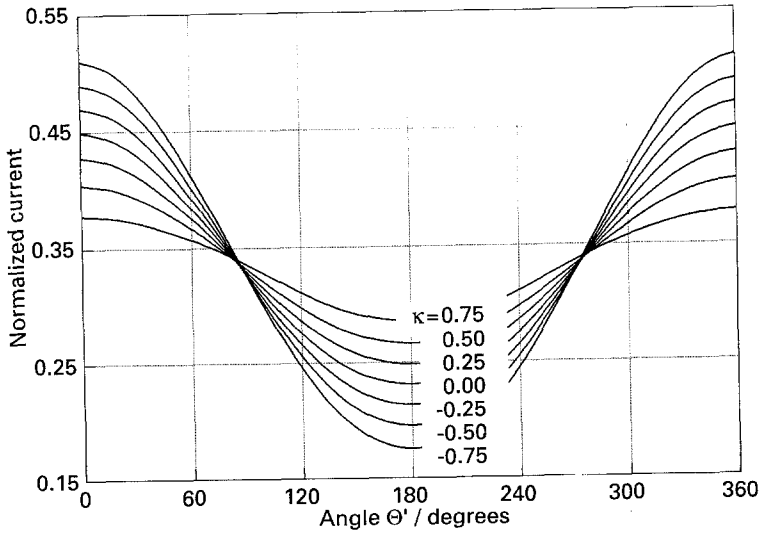

Fig. 7. Influence of the normal velocity component in the directional characteristics (normalized currents) in a planar flow.

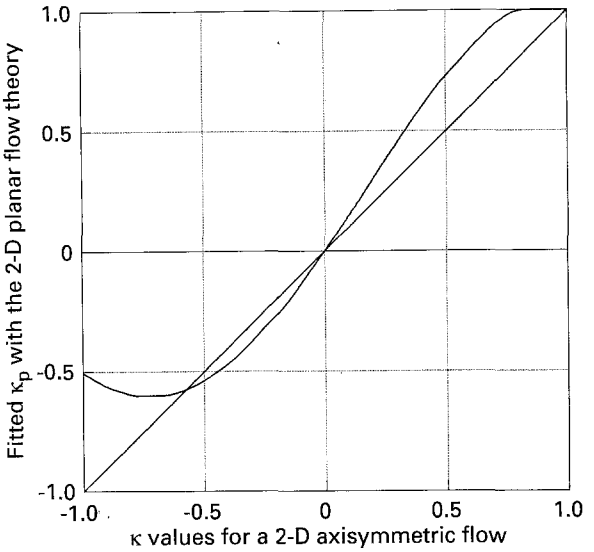

Fig. 8. Comparison of κ_p calculated by means of the planar flow theory with κ defined for anaxisymmetric flow.

plotting the directional characteristics of a real three-segment probe in the stagnation region of an impinging jet cell, and trying to estimate, at the same point, both the parallel and normal velocity components of this flow.

By measuring the total current and the elementary currents relative to each segment, it is possible to measure q and κ separately. They both contain r which is the distance from the stagnation point to the probe centre. Then, by eliminating r between the expressions for q and κ, the first coefficient of the velocity expansion in the normal direction is obtained for this flow:

$$A = \frac{q\kappa}{R}$$

The experimental impinging jet cell, is shown in Fig. 9. It was recently constructed and its mass transfer characteristics assessed by a.c. impedance [12]. The hydraulic circuit consists of the jet cell, a pressure fluctuation damping vessel (vol. 1 dm^3), a gear pump driven by a stepping motor with a maximum controlled flow rate of 30 $ml\,s^{-1}$. The electrolyte flowed through a long tube located at the axis of the vessel and either made of glass (int. diam. 7 mm) or stainless steel (int. diam. 12 mm). The tube was fitted with a nozzle at its extremity. The experiments described here were conducted with the stainless steel tube equipped with a nozzle having an outlet diameter of 6 mm. The jet flow was laminar with a flat velocity profile approaching the theoretical predictions. Under these conditions, the velocity in the jet axis remains uniform over a certain distance from the outlet. On the bottom of the cell, the three-segment probe was mounted on a device having two rotational axes: one off the probe centre, allowing the probe to be moved to different distances from the jet axis, and the second being the probe axis itself, in order to plot the directional characteristics for any value of the jet axis to the probe axis distance, r. The nozzle

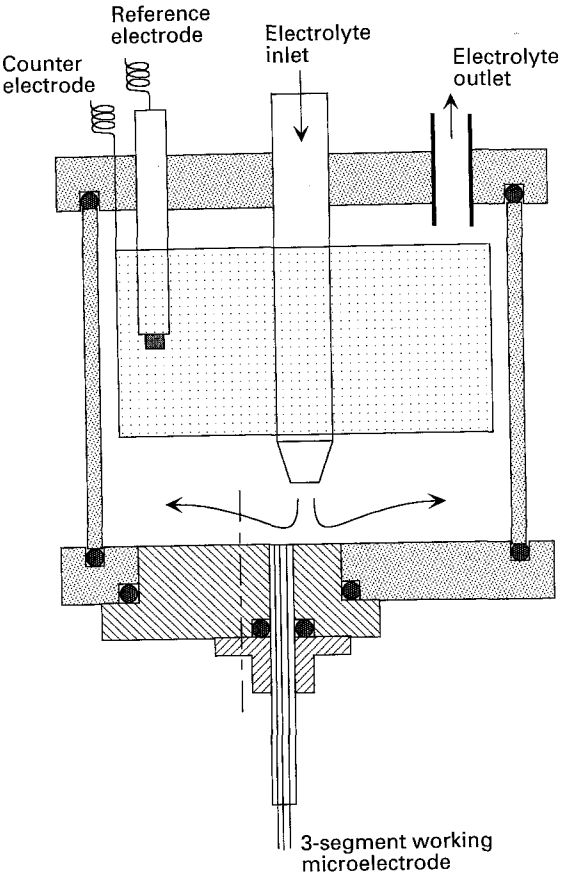

Fig. 9. Scheme of the impinging jet cell.

was positioned 10 mm above the bottom. The jet velocity was 10.6 $cm\,s^{-1}$ which corresponds to a Reynolds number of 640.

The three-segment probe was prepared according to the technique detailed in [2]. Three platinum wires of diameter 0.5 mm were drawn together so as to obtain the final shape of three 120° circular sectors. To decrease the thickness of the insulating gap between the sectors, a variant to the technique previously defined in [2] was used. Instead of rolling a glass wire around each platinum wire before gluing them together so as to prevent their mutual electrical contact, they were initially protected by a cataphoresis deposit. Then, as previously, the wires were glued together and an epoxy resin (Buehler) was poured in a stainless steel tube which served as the counter electrode.

Due to the geometrical imperfections of the microelectrodes, a preliminary calibration was necessary. This was done in a cone and plate device at low velocities which ensured perfectly viscometric conditions and was free from a normal velocity component. Therefore, the basic theory applies [1]. Then, the directional characteristics of each segment (i.e. $I_{i\in\{1,2,3\}} = f_i(\theta)$) were determined, from which the experimental values of the C_m^A coefficients (which differ from the theoretical ones given in Table 1) were calculated. Hence, the E_{im} coefficients for any κ value were assumed to be the same as the theoretical expression of C_m^A was fitted to the experiments to determine the different κ values.

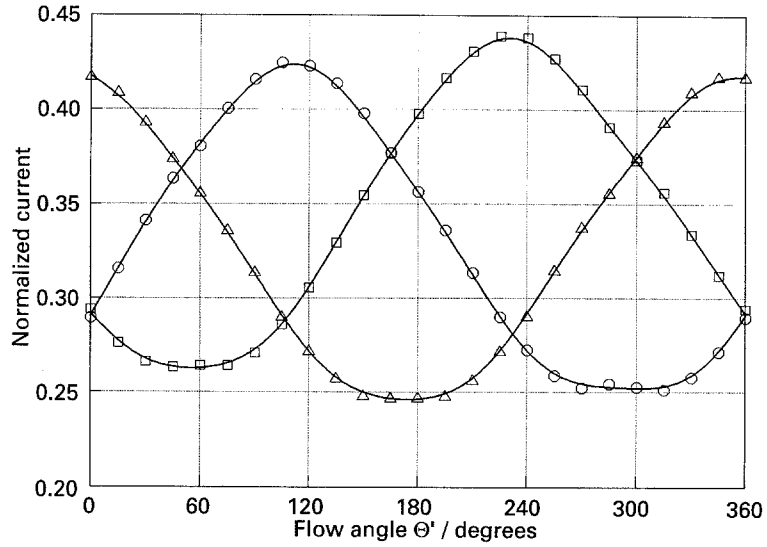

Fig. 10. Directional characteristics of a three-segment probe in the impinging jet cell at 9.3 mm from the stagnation point. ($\kappa = 0$). Probe diameter 0.62 mm.

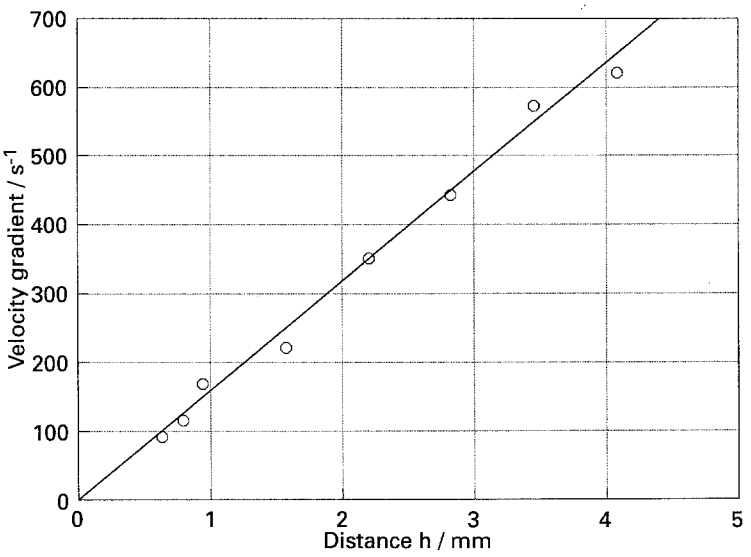

Fig. 11. Velocity gradient as function of the radial coordinate in the stagnation region. Same probe as in Fig. 10.

The test fluid was a 25 mol m^{-3} equimolar potassium ferri/ferrocyanide solution with 500 mol m^{-3} K_2SO_4 as supporting electrolyte. The potential applied on all three segments was −0.7 V, corresponding to the diffusion limiting current for potassium ferricyanide reduction.

From the calibration in the cone-and-plate device, the total current through the three-segment probe with a diameter of 0.62 mm was found to be $I = 6\tau^{1/3}$, where I is the current in μA and τ the velocity gradient in s^{-1}. The calibration curve for $\kappa = 0$ was also obtained in the impinging jet cell at a distance of 9.3 mm from the stagnation point, where the influence of the normal component is

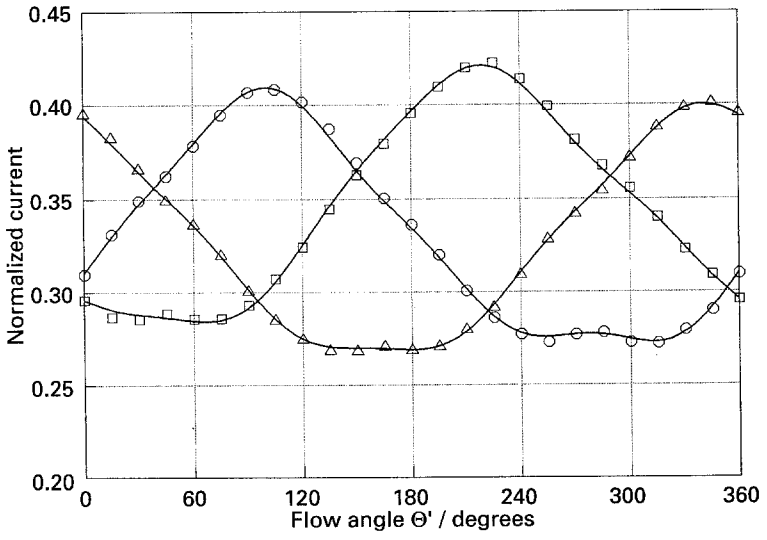

Fig. 12. Directional characteristics of the three-segment probe at $r = 2.8$ mm from the stagnation point. (——) Best fit for $\kappa = 0.21$ with the axisymmetric flow model.

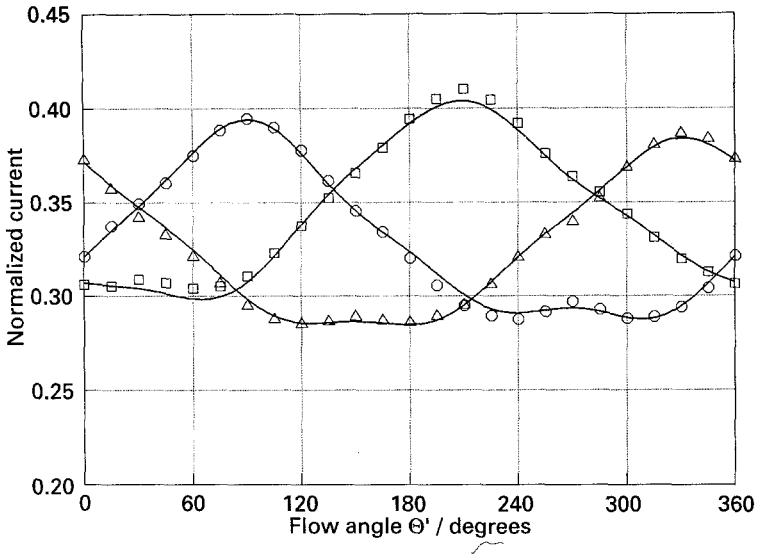

Fig. 13. Directional characteristics of the three-segment probe at $r = 0.95$ mm from the stagnation point. (——) Best for for $\kappa = 0.37$ with the axisymmetric flow model.

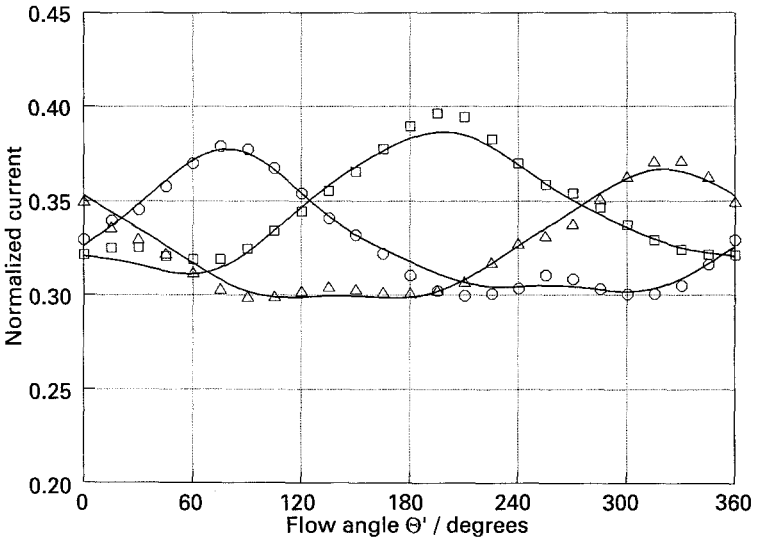

Fig. 14. Directional characteristics of the three-segment probe at $r = 0.8$ mm from the stagnation point. (——) Best fit for $\kappa = 0.52$ with the axisymmetric flow model.

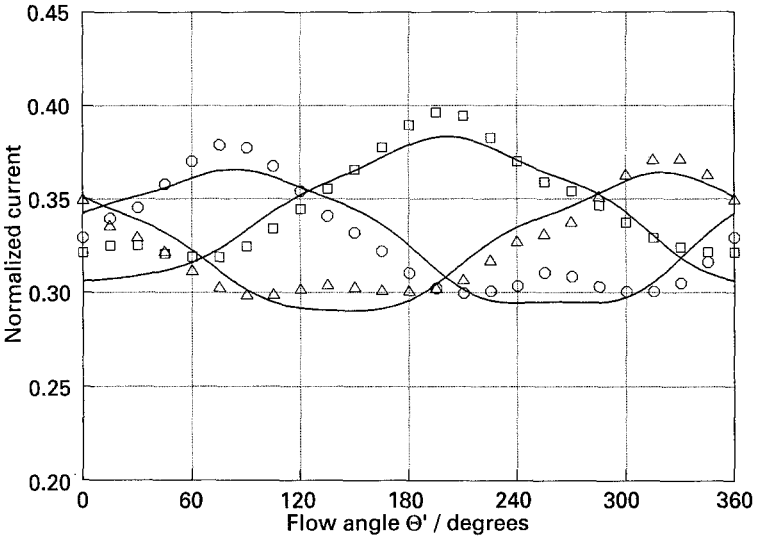

Fig. 15. Same data as in Fig. 14. (——) Best fit for $\kappa = 0.75$ using the planar flow model instead of the axisymmetric flow model.

negligible. The corresponding directional characteristics are shown in Fig. 10. In the stagnation region, the proportionality of the velocity gradient to the radial coordinate was found in agreement with the theory (see Fig. 11).

Figures 12 to 14 show the experimental directional characteristics with the fitted curves leading to the respective κ values of 0.21, 0.37, and 0.52 assuming an axisymmetric flow. These values compared to the respective theoretical values of 0.11, 0.33 and 0.39, obtained as $\kappa = \delta q/q = AR/Ar = R/r$, show only an approximate agreement but do reveal the existence of a normal component. However, for the highest κ value, the use of a planar flow instead of an axisymmetric one gives a poor fitting (see Fig. 15) and a worse value for κ (0.75 instead of 0.52). The

observed difference between experimental and theoretical values is probably due to the geometrical imperfections of the probe with segments of unequal areas and too large insulating gaps.

6. Conclusion

Axisymmetric flow has a greater influence on the directional characteristics of a three-segment probe than planar flow. The difference is particularly important near a stagnation point. In axisymmetric flow with separation, the influence of radial flow prevails over the training effect of the front segment at $\kappa = -0.75$ and the directional characteristics are not so flattened as in the case of planar flow. Preliminary experiments performed on an impinging jet cell in the stagnation region reveal the existence of a normal component but the accuracy of its evaluation is not good due to the deviation from ideal geometry of the fabricated probes. There is a need for a geometrically well-defined probe for quantitative verification of the theory.

Acknowledgements

This work received financial support through the CNRS(MDRI)/CSAV agreements and an individual fellowship of the Ministère de la Recherche et de la Technologie. The authors also acknowledge Dr G. Maurin for his help in the use of the impinging jet cell.

References

[1] O. Wein and V. Sobolik, *Collect. Czech. Chem. Comm.* **52** (1987) 2169–2180.
[2] V. Sobolik, P. Mitschka and T. Menzel, 'Method of manufacture of segmented probe with circular cross-section', *Czech. Patent AO 262 823* (1989).
[3] T. Menzel, V. Sobolik, O. Wein and U. Onken, *Chem. Ing. Tech.* **59** (1987) 492–493.
[4] C. Deslouis, O. Gil and V. Sobolik, *Int. J. Heat Mass Transfer* **33** (1990) 1363–1366.
[5] O. Wein and V. Sobolik, *Collect. Czech. Chem. Comm.* **54** (1989) 3043–3060.
[6] V. Sobolik, O. Wein, O. Gil and B. Tribollet, *Exp. in Fluids* **9** (1990) 43–48.
[7] H. Schlichting, 'Boundary Layer Theory', McGraw Hill, New York (1968) p. 90.
[8] A. Acrivos, *Phys. Fluids*, **3** (1960) 657–658.
[9] J. Newman, 'Electrochemical Systems', Prentice Hall, Englewood Cliffs, NJ (1991) p. 359.
[10] O. Wein, *Coll. Czech. Chem. Commun.* **55** (1990) 2404.
[11] M. A. Lévêque, *Ann. Mines* **13** (1928) 201–299, 305–362, 381–415.
[12] V. Bouet, C. Gabrielli, G. Maurin and H. Takenout, *J. Electroanal. Chem.* **340** (1992) 325–331.